Materials Horizons

COMMUNICATION

View Article Online
View Journal | View Issue

Cite this: *Mater. Horiz.*, 2018, 5, 51

Received 24th August 2017,
Accepted 17th October 2017

DOI: 10.1039/c7mh00676d

rsc.li/materials-horizons

Monitoring crack appearance and healing in coatings with damage self-reporting nanocapsules†

Minghan Hu,[a] Stefan Peil,[a] Yaowen Xing,[a] Diana Döhler,[b] Lucas Caire da Silva,[a] Wolfgang H. Binder,[b] Michael Kappl[a] and Markus B. Bannwarth*[a]

Autonomous highlighting of damage in protective polymer coatings allows on-demand maintenance and enables prolongation of the lifetimes of the coated materials. To monitor the entire cycle of damage occurrence and successful healing, one must be able to visualize both processes and display the current health-state of the coating. Herein, we equipped coatings with nanocapsules that can self-indicate their mechanical micro-damage *via* color development. Hence, whenever the coating was damaged, the capsules broke and highlighted the damaged spot. As a second feature, the color development was reversed and discoloration occurred in the presence of (self-)healing compounds, allowing the user to monitor the healing process. Thus, in the first step, damages were highlighted *via* color "turn-on" and in the subsequent step a propagating healing reaction "turns-off" the damage indication system to trace the healing reaction and allow monitoring of the entire health cycle.

Conceptual insights

The exposure of materials to environmental stress causes damage and can eventually lead to catastrophic failure. Monitoring the intactness of materials, such as polymeric coatings, can provide a warning of impending failure and significantly prolong their lifetimes. In this manuscript, we introduce the novel concept of a health-state monitoring system for coatings that can indicate when damage occurs and, additionally, when it has been healed. To achieve this monitoring system, we integrated capsules that can self-indicate their damage *via* the development of color in the coatings. Hence, when the coating is damaged, the capsules break and the damaged spot is highlighted. As a second feature, the color development is reversed in the presence of (self-)healing compounds to allow tracking of the healing process. Thus, in the first step, damage is highlighted *via* color "turn-on" and, in a subsequent step, a propagating healing reaction "turns off" the damage indication system to trace the healing reaction and allow full control over the healing process. We envision that our reversible self-reporting system can pave the way towards a new generation of materials with multiple autonomous reporting functions to display the current health states of materials – from the occurrence of damage to successful healing.

Polymer coatings can act as protective envelopes around many materials to prolong their lifetimes (*e.g.* preventing corrosion of metals[1,2]) until exposure to environmental stress leads to damage of the coatings and impairment of their protective functions.[3,4] Hence, it is important to detect and repair damages as early as possible. However, minor (nano- or micro-scale) damages are hardly visible, and common coatings do not possess the ability to autonomously highlight cracks to alert the user to impending failure. To endow coatings with an autonomous damage-reporting function, dye-loaded microcapsules have been integrated in polymeric coatings.[5] Upon mechanical damage of the coating and subsequent rupturing of the capsules, the released indicator dye can change its chemical structure *via* UV-light exposure,[6,7] chemical reaction,[8–10] or physical aggregation[11,12] to present a visible or fluorescent signal at the damaged spot. In addition, some bulk polymer materials can change their color upon mechanical stress *via* chemical transformation of the polymers.[13–15] Thus, micro-damage in the coating is autonomously highlighted to initiate maintenance of the coating.

Currently, damage occurring in coatings can be reversibly healed by a number of well-established self-healing systems.[16–19] Thus, self-healing coatings can heal cracks by dynamic formation of reversible chemical bonds,[20–27] by covalent crosslinking polymerization of monomers released from microcapsules[28–30] or by generating radicals during the damage process, which can initiate the repair reaction.[31] Thus, the success of damage healing depends on several factors, such as the distribution of self-healing agents within the coating, the environmental temperature, and the size and depth of the damage. Thus, monitoring the success of damage healing is essential to guarantee the protective function of the coating and to indicate required coating maintenance. Therefore, it is essential to visualize

[a] *Max Planck Institute for Polymer Research Ackermannweg 10, D-55128 Mainz, Germany. E-mail: bannwarth@mpip-mainz.mpg.de*
[b] *Faculty of Natural Science II (Chemistry, Physics and Mathematics), Institute of Chemistry, Division of Technical and Macromolecular Chemistry, Chair of Macromolecular Chemistry, Martin Luther University Halle-Wittenberg von-Danckelmann-Platz 4, D-06120 Halle, Germany*

† Electronic supplementary information (ESI) available. See DOI: 10.1039/c7mh00676d

damage that is not being healed with a self-reporting system. However, when the irreversible damage-reporting capsules described in the literature to date are combined with self-healing coatings, the capsules can highlight the crack even if it is being or has already been healed.[32]

To enable simultaneous monitoring of damages in coatings and their self-healing, the optical damage indication must be reversible. Currently, a hurdle to this reversibility is that the incorporated healing agents cannot deactivate the active indicator to turn off the optical signal. Therefore, it is crucial to create a system that can not only turn on the signal to report the appearance of damage, but can additionally turn off the signal to report that the damage is being healed.

Here, we introduce a nanocapsule-based system for autonomously monitoring the appearance and healing of mechanical micro-damage in polymeric coatings. Our damage appearance and healing monitoring system is schematically illustrated in Fig. 1. First, we designed a three-component nanocapsular system (Fig. 1a) in which the damage-indicating dye is encapsulated within a protective polymer shell which is further coated with a color developer. When the shell is mechanically broken, the released inactive dye (decolored form) becomes active (colored form) by reacting with the color developer. In this manner, the nanocapsules autonomously report their destruction; this system allows spatial and functional separation from the surrounding medium and other capsules, enabling the universal use of this self-reporting nanocapsule-based system to indicate damages in various coatings (Fig. 1b). As an additional feature, in addition to color indication, a defined second reaction between the color indication system and the surrounding medium can be implemented. Thus, the interactions between the dye and the color developer can be reversibly deactivated by different self-healing compounds or byproducts of self-healing reactions. Consequently, the self-reporting capsule-based system can not only turn on its optical signal for sensing cracks in coatings, but can also turn off the signal by interacting with healing agents to highlight only the damage that is not being healed.

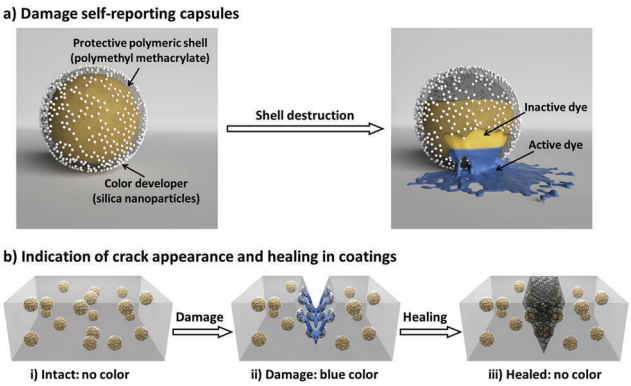

Fig. 1 (a) Scheme of a damage self-reporting capsule. The colorless damage-indicating dye (CVL) is encapsulated in a silica-coated polymer shell. When the capsule shell is broken, the released dye is developed through interaction with silica to afford a deep blue color (CVL^+). (b) Damage self-reporting capsules embedded in a waterborne polymeric coating to indicate crack appearance and self-healing. When mechanical damage occurs, the dye is released and reacts locally with the color developer at the surface of the ruptured capsules to highlight the damaged spot *via* a colorimetric indication. When self-healing agents come in contact with the dye, the color disappears; this lack of visible color enables monitoring of the self-healing reaction.

Crystal violet lactone (CVL) was selected as a color indication dye because of its intense color change capabilities through selective reaction with manifold compounds, which can develop or remove its color.[33,34] Reversible opening of the lactone ring of colorless CVL can be induced through hydrogen bonding (*e.g.* through the silanol groups of silica, see Fig. S1 in the ESI†) to form CVL^+, which has an intense blue color (Fig. 2a, photograph (i) and (ii)). To demonstrate the color development, CVL was dissolved in phenyl acetate and added dropwise onto silica powder. An intense blue color immediately evolved, indicating the conversion of CVL to CVL^+ (see Movie 1, ESI†); this can be monitored by a broad absorption peak with a maximum at λ = 603 nm *via* UV/Vis measurements (Fig. 2b).

In addition to the color developing mechanism, the color deletion mechanism in the presence of various decoloring agents was investigated. Ethanol, diethylenetriamine (DETA) and multivalent alkynes are common self-healing components[28,35,36] or byproducts[37–39] of self-healing reactions; they were found to be suitable as decoloring reagents. To demonstrate the decoloring feature, different amounts of decoloring agent were mixed with CVL^+ which had previously been developed in the presence of silica powder (Fig. 2a, photograph (iii)). The absorption band of the colored CVL^+ at 603 nm decreased with increasing amounts of decoloring agent (Fig. 2c). Although all three agents showed a color-deleting effect on CVL^+, their decoloring kinetics were noticeably different: the multivalent alkyne deleted the blue color in two hours, while DETA and ethanol deleted the color within minutes (see Movie 2–4, ESI†). Additionally, the amounts of decoloring agents that can initiate the color-deleting effects were found to be different (Fig. S3, ESI†). Thus, variations in the color-removing efficiency between the different decoloring agents and CVL^+ or silica are probably related to their different decoloring mechanisms. The strong blue color of CVL^+ is initiated by hydrogen bonding of the relatively acidic hydroxyl groups of silica with the carboxylate groups of CVL^+.[40] Breakage of these hydrogen bonds, and consequent color fading, can be achieved by adding either polar alcohols, such as ethanol, that insert between the silica and the CVL^+,[41] or by adding base. The dependence of the color development on the acid/base equilibrium is apparent from the ^{1}H NMR spectra in solution. As shown in Fig. S4 (ESI†), color developing with HCl causes the expected downfield shift of the aromatic proton signals of CVL due to opening of the lactone ring. Addition of DETA, on the other hand, immediately neutralizes the effect of HCl and quantitatively restores CVL from CVL^+. To understand the color-deleting capability of the multivalent alkyne, it should be noted that the alkyne substitution reaction of trimethylolpropane does not reach 100% completion. Instead, a mixture of mono-, di- and trisubstituted products is obtained (Fig. S8, ESI†). The main product (83 mol%) is the trivalent alkyne; however, the incomplete conversion results in many unsubstituted alcohol groups. To evaluate the color-deleting effect of the

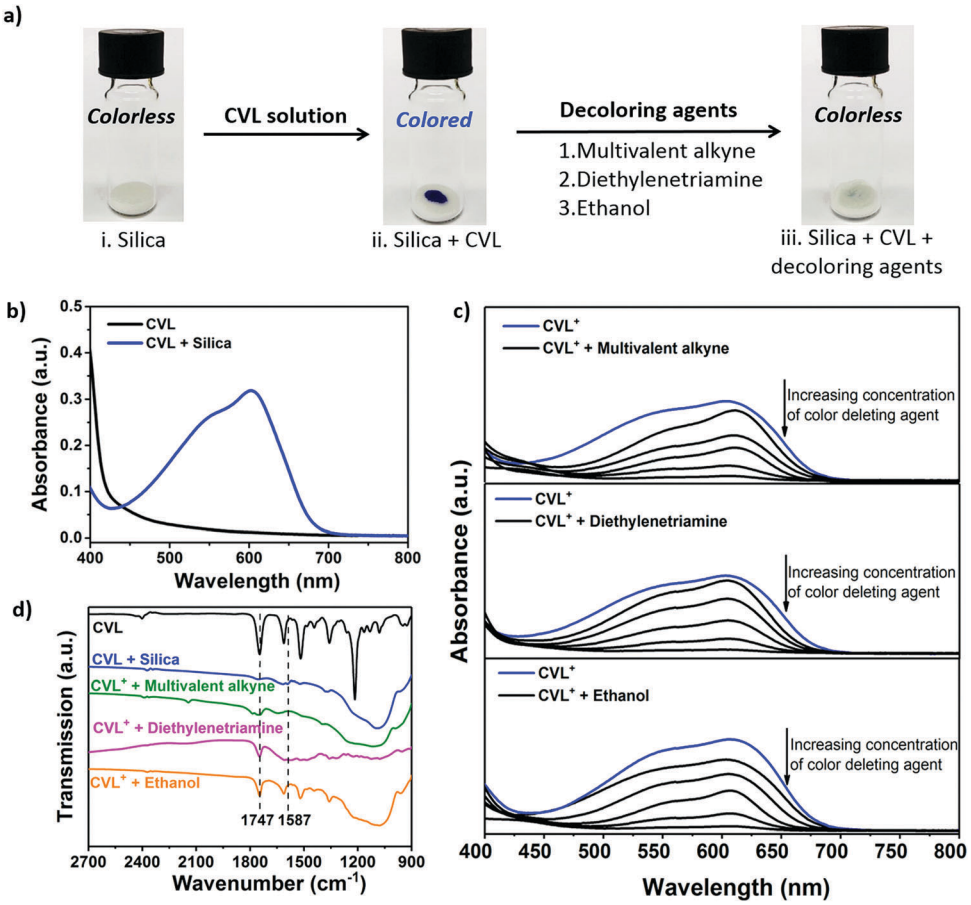

Fig. 2 (a) Color development and color deletion reactions of the dye system. Photographs of (i) silica powder, (ii) a mixture of silica and CVL powder after development of the color and (iii) silica and CVL powder after the addition of different decoloring agents to delete the blue color. (b) UV/Vis spectra of CVL and CVL mixed with silica nanoparticles. (c) UV/Vis spectra of CVL^+ reacted with different amounts of the decoloring agents, namely multivalent alkyne, diethylenetriamine, and ethanol. (d) FTIR spectra of a CVL powder, a mixture of silica and a CVL powder after developing of the color, and CVL^+ with three decoloring agents (multivalent alkyne, diethylenetriamine, and ethanol).

hydroxyl groups of the partially alkyne-substituted trimethylolpropane, we added trimethylolpropane to a silica/CVL mixture (CVL in its open ring structure, with blue color). As a result, the trimethylolpropane quickly deleted the color. As an additional experiment, we investigated whether propargyl bromide (with its alkyne group) could delete the color; we found that it has no color-deleting effect. Thus, the hydroxyl groups of trimethylolpropane (and its mono- and disubstituted forms) delete the color. Most probably, the hydroxyl groups of the alcohols can insert between the CVL and silica to break their hydrogen bonds. In contrast to the relatively acidic hydroxyl group of the silica ($pK_a \approx 6.8$ for small particles),[42] the much less acidic alcoholic hydroxyl group ($pK_a \approx 17$) is less likely to force a ring opening reaction and enables closure of the ring (color deletion). Thus, when a mixture of mono-, di- and trialkyne-containing methylolpropanes is used for the self-healing reaction, two functions are provided: (1) The alkyne groups will react with azides and form a polymer network; (2) the leftover hydroxyl groups, which are positioned as side chains of the formed polymer network, will delete the color of the CVL. Therefore, the color deletion remains even after the self-healing is completed.

Additionally, the hydrogen bonding ability between the dye, the hydroxyl groups of the silica, and the decoloring agents was investigated *via* FTIR spectroscopy (Fig. 2d). The pure CVL shows a band at 1747 cm^{-1} due to the vibration of the C=O group of the lactone ring. When silica reacts with CVL, a new band arises in the spectrum of CVL^+ at 1587 cm^{-1}; this can be ascribed to the carboxylate group of the opened lactone ring. This band disappears when the color-deleting agents interact with CVL^+, indicating the closure of the lactone ring.[43] Thus, the color of CVL can be developed with silica and can be deleted by self-healing agents or byproducts of the healing reaction.

In order to design the above-described damage self-reporting capsule, three compounds were engineered together in one nanomaterial. The inactive and colorless CVL was encapsulated in a protective poly(methyl methacrylate) (PMMA) shell, and the surface of the capsule was decorated with color-developing silica nanoparticles. The spatial separation of CVL and silica by the protective polymer shell was achieved in a one-step miniemulsion solvent-evaporation process (details in Experimental section and Fig. S5, ESI†), in which the silica particles function as a Pickering stabilizer. At the beginning of

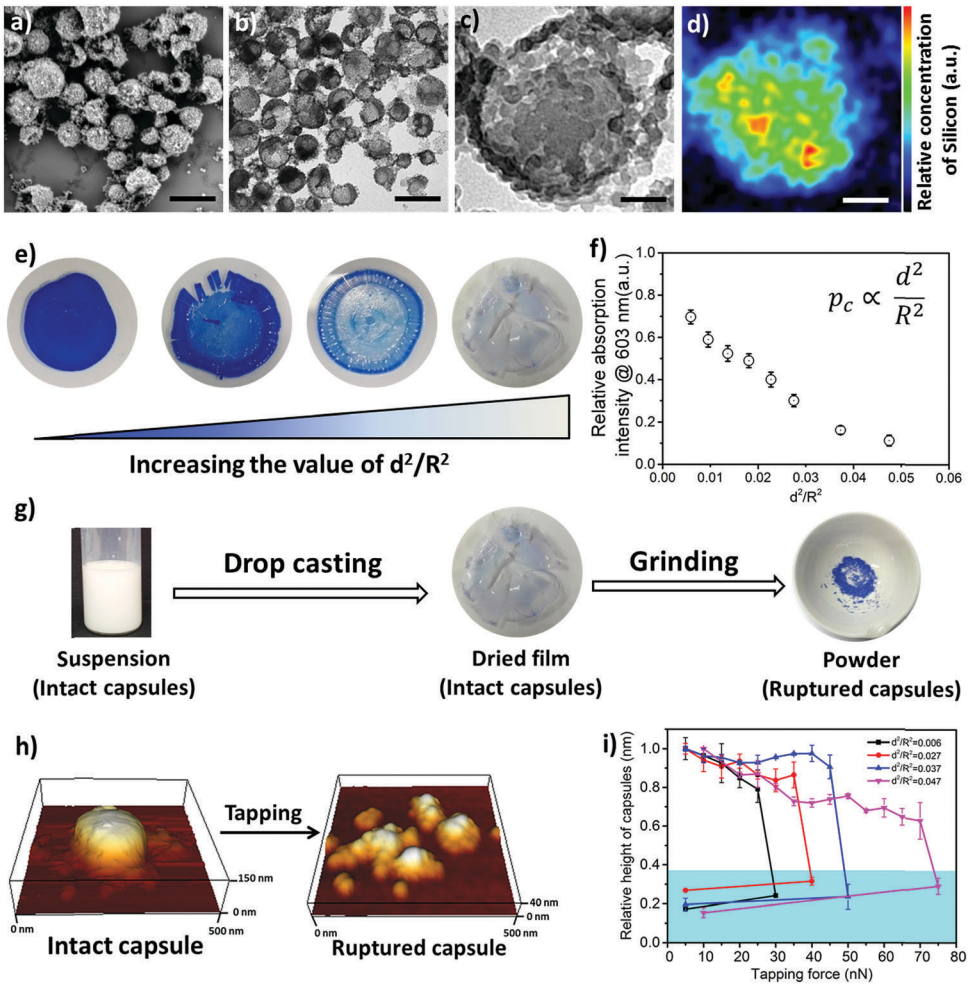

Fig. 3 Tuning of the color response and mechanical stability of the damage self-reporting nanocapsules. (a) SEM image, (b) and (c) TEM images and (d) SEM–EDX silicon mapping of the fabricated nanocapsules (scale bars are 300 nm, 300 nm, 100 nm, and 100 nm, respectively). (e) Optical photographs of dried capsule suspensions with different critical buckling pressures. (f) Absorption intensities at λ = 603 nm of the dried capsules as a function of their $\frac{d^2}{R^2}$ values as determined by UV/Vis measurements. (g) A suspension of the capsules at the highest critical buckling pressure $\left(\frac{d^2}{R^2} = 0.047\right)$ was dried without the development of blue color. When these dried capsules were ground with a pestle, a strong blue color developed. (h) AFM height images of a capsule $\left(\frac{d^2}{R^2} = 0.006\right)$ in suspension before and after rupture. (i) Changes in the normalized apparent heights of the capsules with increasing set-point force. The area indicated in cyan marks the values measured after rupturing of the capsules.

the solvent-evaporation process, PMMA and CVL were homogeneously dissolved in a mixture of chloroform and phenylacetate. During the evaporation of the chloroform, the PMMA became insoluble and the phase separated from the phenyl acetate to form the solid capsule shell, while the CVL remained dissolved in phenyl acetate to consequently create the liquid core. The raspberry-like surface topology of the capsules was observed *via* scanning electron microscope (SEM) imaging (Fig. 3a), and their core–shell morphology was observed *via* transmission electron microscope (TEM) imaging (Fig. 3b and c). The silica nanoparticles cover the shell of the nanocapsules, as shown by the SEM–EDX mapping image (Fig. 3d).

For successful implementation of the prepared nanocapsules as damage-indication systems in coatings, their mechanical response must be tuned so that they do not break in suspension or during the process of embedding in the coating, but exclusively when they are exposed to air (*e.g.* through a crack in the coating). The mechanical stability of micro-/submicrocapsules is related to the critical buckling pressure (p_c) of spherical capsules,[44] which mainly relates to the radius (R) and shell thickness (d) of the capsules as follows:

$$p_c \propto \frac{d^2}{R^2} \quad (1)$$

To further understand the mechanical stability of the capsules, different submicro-/nanocapsules with different p_c values were prepared. By varying the silica concentration, the amount of PMMA, and the sonication amplitude, the hydrodynamic

diameter of the capsules can be tuned between approximately 200 and 1100 nm and the shell thicknesses can be tuned between approximately 10 and 120 nm (Table S1, ESI†). First, the stability of the capsules was tested by drying the capsules under ambient conditions. The white suspensions of capsules were drop-casted on glass slides and dried for several hours at room temperature. During drying of the dispersions, capillary forces between the particles will occur in two ways: first, during recession of the air–water interface from the outmost layer of particles down to the substrate, and second, during drying of the remaining menisci. These forces can cause the capsules to collapse during drying, depending on their mechanical stability, and a blue color then develops. After drying, the capsules with different shell thicknesses developed varying intensities of blue color (Fig. 3e). We used eqn (1) to evaluate the critical buckling pressures of the capsules[44] and tune the color development. As shown in Fig. 3f, the color intensity decreased with increasing value of $\frac{d^2}{R^2}$. The capsules with $\frac{d^2}{R^2} < 0.030$ developed an intense blue color, indicating that the shells had been damaged during the drying process owing to their weak shell stability (Fig. S6a, ESI†). However, capsules with $\frac{d^2}{R^2} > 0.030$ showed no blue color and displayed a white color after drying, indicating that the capsules were able to resist the drying process (Fig. S6b, ESI†). To further test the robustness of the capsules and to demonstrate their capability to still develop a blue color upon breaking, the dried capsules with higher critical buckling pressure $\left(\frac{d^2}{R^2} = 0.047\right)$ were subsequently ground with a pestle. After grinding, the submicrocapsules developed a blue color, indicating the destruction of the shell and the color development ability of the submicrocapsules (Fig. 3g). To estimate the force needed to break the capsules during the drying process, the capillary force (F_c) can be calculated according to eqn (S2) in the ESI.† For example, the capillary force for capsules with a diameter of 300 nm can be calculated as F_c = 65 nN (eqn (S4), ESI†). To investigate if this calculated capillary force is enough to break the capsules, we performed atomic force microscopy (AFM) measurements in which we applied a certain force to one capsule in an aqueous environment. With AFM, a defined force can be applied directly with the tip of the cantilever on a single capsule until it breaks (Fig. 3h). Fig. 3i further shows that the apparent height of the capsules decreases when they are imaged using an increasing contact force. When the contact force reached a certain threshold, the apparent height of the capsules dramatically declined to a very low value; this remained constant after the initial low contact force was applied again, indicating that the capsule had been irreversibly ruptured. Hence, the rupture forces of the investigated capsules can be precisely measured (for the investigated cases, 30 to 75 nN) and fine-tuned depending on the shell thickness. The determined forces are in good agreement with the capillary force that occurs on the capsules during drying (as calculated from eqn (2), ESI†).

To demonstrate the capability of the damage self-reporting capsules for micro-crack indication in coatings, we combined the nanocapsules with a low critical bulking pressure $\left(\frac{d^2}{R^2} = 0.006\right)$ that break upon exposure to air with a commercially available waterborne polymer coating (approx. 100 μm thick). Therefore, the nanocapsule suspension was firstly coated on a glass slide, pre-dried and sealed with the commercial coating to avoid breakage of the capsules (for details, see the Experimental section). Introduction of the capsules to the commercial coating caused only a minor decrease of the transparency of the coating, which retained its optical properties (Fig. S10 and S11, ESI†). Micro-cracks were artificially induced by scratching with a razor blade and were observed by stereomicroscopy and SEM. While the control coating without any nanocapsules showed no color development (Fig. 4a), the coating containing nanocapsules highlighted the induced micro-cracks *via* the appearance of a strong blue color (Fig. 4b). Hence, the described system autonomously reports the damaging of a coating upon mechanical disintegration. By chemically modifying the release properties of the capsules (*e.g.* redox-responsive release),[45] other types of damage, such as redox-disintegration of the coating, can be detected in the future as well.

In the next step, the chemical response of the coating system with self-healing compounds was tested to investigate whether only non-healed damage can be reported. Therefore, the reversibility of the color development process through the reaction with self-healing compounds was demonstrated by analyzing the color-deletion properties of CVL^+ in the presence of multivalent alkyne and azide (self-healing monomers), which can form a polymer network suitable for self-healing *via* ''click'' chemistry at room temperature and achieve a self-healing efficiency of nearly 100% after 48 h.[28] In addition to the two ''click'' monomers, we added a $Cu^{(I)}Br(PPh_3)_3$ catalyst to significantly accelerate the healing reaction at lower temperatures (Fig. S7, ESI†). When multivalent alkyne, multivalent azide and $Cu^{(I)}Br(PPh_3)_3$ were added into the strongly blue colored crack, the color slowly vanished in a time frame of two days until it finally completely disappeared. Simultaneously, the crack was healed (Fig. 4c). Hence, the capsule system can be applied to autonomously indicate the ''click''-induced healing of the coating when the blue color is reversibly deleted. In addition to the ''click''-chemistry healing system, we showed that other classes of self-healing reactions, including the epoxy-amine[36] and PDMS self-healing[37] systems, can turn off the optical signal and therefore indicate a successful self-healing reaction. In the case of the epoxy-amine self-healing system, the free amine groups of the healing agents delete the color (see Movie 3, ESI†); meanwhile, in the case of the PDMS self-healing system, the color of CVL^+ is deleted by the ethanol that is produced during the healing reaction (see Movie 4, ESI†).

In summary, we have developed a reversible damage self-reporting nanocapsular system, which was subsequently used to monitor micro-crack appearance and healing in coatings. Therefore, a three-component capsule was designed which contains an inactive dye in the liquid core, a protective polymer shell and color-developing silica nanoparticles on its surface. Breakage of the shell enables autonomous destruction-reporting

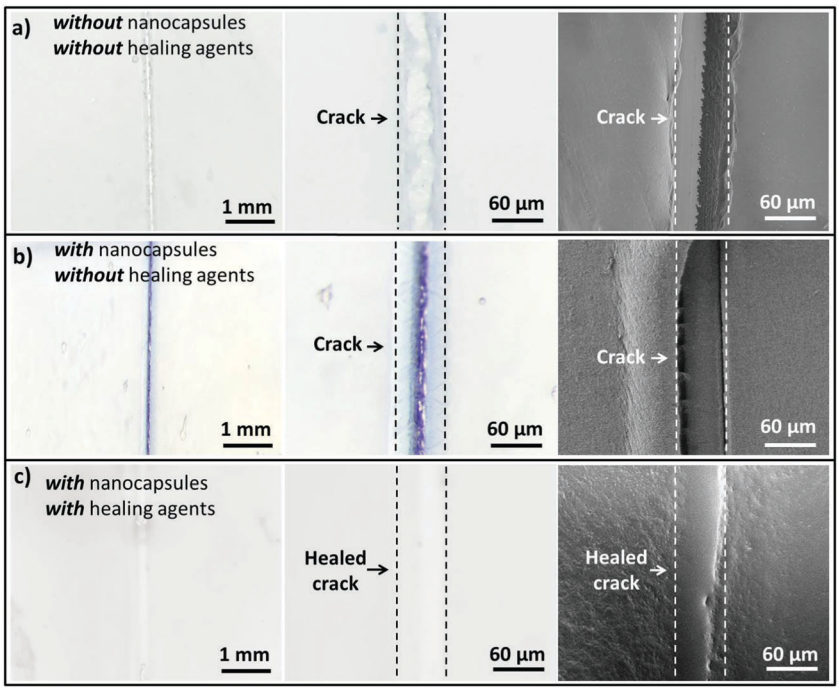

Fig. 4 Autonomous colorimetric indication of crack appearance and color deletion to report crack healing. Optical photographs (left and middle column) and SEM images (right column) of a micro-crack in a polymeric coating in the (a) absence and (b) presence of damage self-reporting nanocapsules. (c) The colored micro-crack is healed and reversibly becomes colorless when in contact with the self-healing system composed of multivalent alkyne, multivalent azide, and $Cu^{(I)}Br(PPh_3)_3$.

via development of an intense blue color. When the capsules are embedded in coatings, they break upon damage of the coating and highlight the damaged spots. The visually highlighted spots can be erased through interaction of the dye with different self-healing compounds or byproducts of self-healing reactions and subsequent color deletion. Hence, the system can be applied to monitor the appearance and healing of damage in coatings by introducing a second type of reported capsular[28,36] or vascular systems[46] to release the healing compounds (alkyne and azide, epoxy amine, PDMS, *etc.*). We envision that our reversible self-reporting system with high versatility can be applied in a new generation of self-reporting coatings which have multiple autonomous functions to monitor the whole health cycle of artificial materials.

Experimental section

Materials

Crystal violet lactone (CVL, 97%) was obtained from Alfa Aesar (USA), and phenyl acetate was obtained from Sigma-Aldrich (USA). Poly(methyl methacrylate) (M_w is 120 000 g mol^{-1} as determined by GPC) and LUDOX® HS-30 (30 wt% dispersion) were obtained from Sigma-Aldrich (USA), chloroform (> 99%) was obtained from Acros Organics (Belgium), and aqueous HCl solution (1 mol L^{-1}) was obtained from Carl Roth (Germany). For the model coating experiment, a waterborne polymeric coating (Mowilith® DHS S1, Celanese, Germany) was kindly donated by Celanese Corporation and was used as the coating matrix material. The multivalent azide and the multivalent alkyne (equimolar ratio) and $Cu^{(I)}Br(PPh_3)_3$ (1 mol%, 98%, Sigma-Aldrich, USA) were used for the damage self-healing tests. The synthesis of these healing chemicals[35] is briefly described as follows: for the synthesis of the multivalent alkyne (trimethylolpropane tripropargyl ether) (Fig. S8, ESI†), trimethylolpropane (97%, Sigma-Aldrich, USA) was converted with propargyl bromide (80% in toluene, Sigma-Aldrich, USA) at 60 °C for 41 hours in the presence of sodium hydroxide (99%, Grüssing, Germany) as a deprotonating agent and tetra-*n*-butylammonium bromide (99%, TCI, Belgium) as a phase transfer catalyst; the crude product was purified by column chromatography. The structures of the multivalent alkyne were determined with a SHIMADZU GCMS-QP2010 gas chromatograph mass spectrometer. The multivalent azide (((2-((2-acetoxy-3-azidopropoxy)methyl)-2-ethylpropane-1,3-diyl)bis(oxy))bis(3-azidopropane-1,2-diyl) diacetate) was prepared in a two-step synthesis (Fig. S9, ESI†). Therefore, ring opening of trimethylolpropane triglycidyl ether (technical grade, Sigma-Aldrich USA) and the subsequent azidation reaction were performed in methanol (99.8%, Sigma-Aldrich, USA) under refluxing conditions within 24 h in the presence of sodium azide (99.5%, Sigma-Aldrich, USA) followed by acetylation with acetic anhydride (99%, Sigma-Aldrich, USA) which proceeded over 89 hours at room temperature in DMF (99%, Grüssing, Germany). Diethylenetriamine (99%, Sigma-Aldrich, USA) and ethanol (> 99.5%, Sigma-Aldrich, USA) were used for the color deletion tests.

Preparation of damage self-reporting nanocapsules

The three-component nanocapsules were fabricated by combining a Pickering emulsion with the solvent evaporation technique.[47]

Varied amounts of poly(methyl methacrylate) (PMMA) (300 to 1200 mg; for detailed information, see Table S1, ESI†) were first dissolved in 5 g chloroform. Then, 100 mg crystal violet lactone (CVL) was dissolved in 1 g phenyl acetate in a separate vessel. The CVL and PMMA solutions were mixed together in a vessel as the oil phase. Varied amounts (2.4 g, 3.2 g and 4.8 g) of LUDOX® HS-30 as an emulsion stabilizer were added to 16.8 g of distilled water as the continuous phase. The combined phases were mixed using a vortex for two minutes. The pH of the pre-emulsion was adjusted to 8.0 by adding 1 M HCl solution. An ultrasonification tip was used to form the oil in water emulsion under ice bath cooling (d(tip) = 1/2 inch; 30% or 50% amplitude; 30 s pulse, 10 s pause; 3 min). The resulting emulsion was rapidly transferred to a preheated oil bath at 40 °C and stirred at 1000 rpm for 16 hours to evaporate the chloroform.

Coating fabrication

1 mL of the fabricated nanocapsule dispersion (0.3 g of PMMA and 3.2 g of silica were used; the applied ultrasound amplitude was 50%) was centrifuged at 5000 rpm for 15 minutes. Then, the supernatant was removed and the remaining slurry was coated carefully on the surface of a glass slide. After 1 min of pre-drying at room temperature (the capsule suspension should not be dried completely; otherwise, some capsules can prematurely break, resulting in a pale blue color in the final coating layer), 1 g of Mowilith® DHS S1 was coated on top of the capsules as a protective layer. Then, the coating was dried overnight at room temperature. The coating thickness was 96 ± 12 μm (measured by a thickness gage from Mitutoyo company, Japan). For the mechanical damage tests, a razor blade (Stanley 28-510) was used to scratch the coating layer and to form a micro-crack. For the damage healing test, the combined healing agents, namely a multivalent azide, a multivalent alkyne and $Cu^{(I)}Br(PPh_3)_3$ as a catalyst, were placed onto the damaged spot to heal the crack for 48 h at room temperature.

Characterizations

The hydrodynamic diameter of the nanocapsules was measured by DLS (Nano-Zetasizer, Malvern Instruments, UK) at 20 °C under a scattering angle of 90° at λ = 633 nm. The morphologies of the nanocapsules were observed by transmission electron microscopy (TEM, JEOL JEM1400, Japan) and scanning electron microscopy (SEM, Hitachi SU8000, Japan). Before the electron microscopy measurements, 5 μL of diluted dispersion were coated on a silicon wafer (SEM measurement) or 400-mesh copper grid (TEM measurement) and dried at room temperature. The topographies of the fabricated capsules in liquid and air environments were measured using a JPK Nanowizard 3 AFM (JPK Instruments, Berlin, Germany) using Quantitative Imaging mode. In this operation mode, data are acquired by recording the force *vs.* distance curves for each image pixel position. From this data set, the height profile of a sample can be reconstructed by taking the distance at which the repulsive force between the tip and the sample reaches a fixed value (force set-point). For deformable samples, this will result in an apparent sample height value that depends on the selected force set-point and the stiffness of the sample. We chose this imaging mode because the adherence of the capsules in liquid to the silicon wafer was too weak to avoid lateral drift of capsules during intermittent contact (tapping) mode imaging. The spring constant of the cantilevers (OMCL-AC240TS-R3, Olympus, Japan) was determined by the thermal tune method. For the measurements in liquid, a starting set-point force of 5 nN was used; the force was then increased in steps of 5 nN until a critical force was reached at which the capsules collapsed. For the measurements in air, the set-point force was 5 nN. All the experiments were carried out at room temperature (20 °C). For chemical analysis of the shells of the capsules, the SU8000 with an energy dispersive x-ray spectrometer (EDX) was used to measure the content of silicon and carbon. Ultraviolet/visible (UV/Vis) spectra of CVL and CVL^+ with different chemicals (color developing or deleting agents) were obtained using a Perkin Elmer Lambda 25 spectrometer. The transparencies of the coating layer without and with capsules were measured by UV/Vis spectroscopy (wavelength range of 350 to 800 nm). Lactone ring opening and closure were studied by Fourier transform infrared spectroscopy (FTIR) and nuclear magnetic resonance (NMR) spectroscopy. Powder samples and KBr were ground to prepare pellets for FTIR measurements. Solution ^{1}H NMR spectra were acquired using a Bruker Avance spectrometer operating at 300 MHz. All chemical shifts were referenced to the residual proton signals from acetone-d_6 (2.05 ppm). The damage appearance and healing of the coatings were investigated with a Zeiss Axiophot stereomicroscope (Carl-Zeiss Microscopy GmbH, Germany) equipped with a digital camera. Differential scanning calorimetry (DSC) investigations were performed on a 204F1/ASC Phönix (Netzsch, nitrogen flow of 20 mL min^{-1}) in a temperature range from −20 °C to 250 °C with heating rates of 5, 10, 15 and 20 K min^{-1}; alumina crucibles and lids were used.

Conflicts of interest

There are no conflicts of interest to declare.

Acknowledgements

The authors are grateful for the support of the Max Planck Society. M. H. and X. Y. acknowledge the China Scholarship Council for their graduate scholarships. W. H. B. and D. D. acknowledge GRANT DFG BI 1337/8-2 (within SPP 1568 ''Design and Generic Principles of Self-Healing Materials''), and D. D. additionally acknowledges support from the DFG Young Research GRANT SHE-STARS (within SPP 1568 ''Design and Generic Principles of Self-Healing Materials''). We are thankful to Celanese Corporation for kindly donating the coating materials. We gratefully thank E. Muth for FTIR support, G. Glasser for helping with the SEM imaging and SEM–EDX mapping, S. Schuhmacher for assistance with graphics and Prof. Dr K. Landfester for fruitful discussions and carefully reading the paper. Open Access funding provided by the Max Planck Society.

References

1 T. H. Tran, A. Vimalanandan, G. Genchev, J. Fickert, K. Landfester, D. Crespy and M. Rohwerder, *Adv. Mater.*, 2015, **27**, 3825.
2 A. Vimalanandan, L. P. Lv, T. H. Tran, K. Landfester, D. Crespy and M. Rohwerder, *Adv. Mater.*, 2013, **25**, 6980.
3 D. Shchukin and H. Möhwald, *Science*, 2013, **341**, 1458.
4 D. C. Leslie, A. Waterhouse, J. B. Berthet, T. M. Valentin, A. L. Watters, A. Jain, P. Kim, B. D. Hatton, A. Nedder and K. Donovan, *Nat. Biotechnol.*, 2014, **32**, 1134.
5 J. F. Patrick, M. J. Robb, N. R. Sottos, J. S. Moore and S. R. White, *Nature*, 2016, **540**, 363.
6 B. Di Credico, G. Griffini, M. Levi and S. Turri, *ACS Appl. Mater. Interfaces*, 2013, **5**, 6628.
7 Y.-K. Song, K.-H. Lee, D.-M. Kim and C.-M. Chung, *Sens. Actuators, B*, 2016, **222**, 1159.
8 S. A. Odom, A. C. Jackson, A. M. Prokup, S. Chayanupatkul, N. R. Sottos, S. R. White and J. S. Moore, *ACS Appl. Mater. Interfaces*, 2011, **3**, 4547.
9 W. Li, C. C. Matthews, K. Yang, M. T. Odarczenko, S. R. White and N. R. Sottos, *Adv. Mater.*, 2016, **28**, 2189.
10 D. Döhler, S. Rana, H. Rupp, H. Bergmann, S. Behzadi, D. Crespy and W. H. Binder, *Chem. Commun.*, 2016, **52**, 11076.
11 M. J. Robb, W. Li, R. C. Gergely, C. C. Matthews, S. R. White, N. R. Sottos and J. S. Moore, *ACS Cent. Sci.*, 2016, **2**, 598.
12 Y. K. Song, B. Kim, T. H. Lee, J. C. Kim, J. H. Nam, S. M. Noh and Y. I. Park, *Macromol. Rapid Commun.*, 2017, **38**, 1600657.
13 D. A. Davis, A. Hamilton, J. Yang, L. D. Cremar, D. Van Gough, S. L. Potisek, M. T. Ong, P. V. Braun, T. J. Martínez and S. R. White, *Nature*, 2009, **459**, 68.
14 G. R. Gossweiler, G. B. Hewage, G. Soriano, Q. Wang, G. W. Welshofer, X. Zhao and S. L. Craig, *ACS Macro Lett.*, 2014, **3**, 216.
15 D. Ramachandran, F. Liu and M. W. Urban, *RSC Adv.*, 2012, **2**, 135.
16 M. Samadzadeh, S. H. Boura, M. Peikari, S. Kasiriha and A. Ashrafi, *Prog. Org. Coat.*, 2010, **68**, 159.
17 C. E. Diesendruck, N. R. Sottos, J. S. Moore and S. R. White, *Angew. Chem., Int. Ed.*, 2015, **54**, 10428.
18 P. Michael, D. Doehler and W. H. Binder, *Polymer*, 2015, **69**, 216.
19 K. Kratz, A. Narasimhan, R. Tangirala, S. C. Moon, R. Revanur, S. Kundu, H. S. Kim, A. J. Crosby, R. P. Russell, T. Emrick, G. Kolmakov and A. C. Balazs, *Nat. Nanotechnol.*, 2012, **7**(2), 87–90.
20 N. Roy, B. Bruchmann and J.-M. Lehn, *Chem. Soc. Rev.*, 2015, **44**, 3786.
21 F. Herbst, D. Döhler, P. Michael and W. H. Binder, *Macromol. Rapid Commun.*, 2013, **34**, 203.
22 S. Chen and W. H. Binder, *Acc. Chem. Res.*, 2016, **49**, 1409.
23 X. Chen, M. A. Dam, K. Ono, A. Mal, H. Shen, S. R. Nutt, K. Sheran and F. Wudl, *Science*, 2002, **295**, 1698.
24 P. Cordier, F. Tournilhac, C. Soulié-Ziakovic and L. Leibler, *Nature*, 2008, **451**, 977.
25 M. Burnworth, L. Tang, J. R. Kumpfer, A. J. Duncan, F. L. Beyer, G. L. Fiore, S. J. Rowan and C. Weder, *Nature*, 2011, **472**, 334.
26 Z. Wang and M. W. Urban, *Polym. Chem.*, 2013, **4**, 4897.
27 Z. Wang, Y. Yang, R. Burtovyy, I. Luzinov and M. W. Urban, *J. Mater. Chem. A*, 2014, **2**, 15527.
28 S. Rana, D. Döhler, A. S. Nia, M. Nasir, M. Beiner and W. H. Binder, *Macromol. Rapid Commun.*, 2016, **37**, 1715.
29 S. Y. An, D. Arunbabu, S. M. Noh, Y. K. Song and J. K. Oh, *Chem. Commun.*, 2015, **51**, 13058.
30 H. Jin, C. L. Mangun, A. S. Griffin, J. S. Moore, N. R. Sottos and S. R. White, *Adv. Mater.*, 2014, **26**, 282.
31 B. Ghosh and M. W. Urban, *Science*, 2009, **323**, 1458.
32 Y. Guo, L. Chen, D. Xu, J. Zhong, G. Yue, D. Astruc, M. Shuai and P. Zhao, *RSC Adv.*, 2016, **6**, 65067.
33 O. Panák, M. Držková, M. Kaplanová, U. Novak and M. K. Gunde, *Dyes and Pigments*, 2017, **136**, 382.
34 A. Raditoiu, V. Raditoiu, C. A. Nicolae, M. F. Raduly, V. Amariutei and L. E. Wagner, *Dyes and Pigments*, 2016, **134**, 69.
35 A. S. Nia, S. Rana, D. Döhler, W. Osim and W. H. Binder, *Polymer*, 2015, **79**, 21.
36 H. Jin, C. L. Mangun, D. S. Stradley, J. S. Moore, N. R. Sottos and S. R. White, *Polymer*, 2012, **53**, 581.
37 S. H. Cho, H. M. Andersson, S. R. White, N. R. Sottos and P. V. Braun, *Adv. Mater.*, 2006, **18**, 997.
38 M. W. Keller, S. R. White and N. R. Sottos, *Adv. Funct. Mater.*, 2007, **17**, 2399.
39 S. H. Cho, S. R. White and P. V. Braun, *Adv. Mater.*, 2009, **21**, 645.
40 K. Ichimura, A. Funabiki, K.-i. Aoki and H. Akiyama, *Langmuir*, 2008, **24**, 6470.
41 Y. Zhang, J. Dong, H. Sun, B. Yu, Z. Zhu, J. Zhang and A. Wang, *ACS Appl. Mater. Interfaces*, 2016, **8**, 27346.
42 D. J. Belton, O. Deschaume and C. C. Perry, *FEBS J.*, 2012, **279**, 1710.
43 D. C. MacLaren and M. A. White, *J. Mater. Chem.*, 2003, **13**, 1695.
44 A. Fery and R. Weinkamer, *Polymer*, 2007, **48**, 7221.
45 L.-P. Lv, Y. Zhao, N. Vilbrandt, M. Gallei, A. Vimalanandan, M. Rohwerder, K. Landfester and D. Crespy, *J. Am. Chem. Soc.*, 2013, **135**, 14198.
46 A. R. Hamilton, N. R. Sottos and S. R. White, *Adv. Mater.*, 2010, **22**, 5159.
47 A. Schrade, Z. Cao, K. Landfester and U. Ziener, *Langmuir*, 2011, **27**, 6689.

